

Article

Practical Methodology for Evaluating Mining Front Stability Based on the Diametrical Core Deformation Technique

Yizhuo Li *  and Hani S. Mitri 

Department of Mining and Materials Engineering, McGill University, Montreal, QC H3A 0E8, Canada

* Correspondence: yizhuo.li@mail.mcgill.ca

Abstract: The state of stress in a mining front constantly changes with mining activities. In a recent study, the authors developed and verified with laboratory measurements an analytical model for the calculation of mining-induced stresses based on measuring the deformations of a diamond drill rock core extracted perpendicular to the mining front or face. The method is called diametrical core deformation technique (DCDT). In this study, the DCDT is used in combination with 3D numerical modelling to develop a practical methodology for the assessment of mining face stability. To demonstrate the methodology, a diamond drill rock core was retrieved from an access drift face 530 m below the surface of an underground mine in northern Quebec. The state of stress in the mining front is estimated from the DCDT and used to adjust the orientation and principal stress magnitudes in the local area around the access drift in a 3D linear-elastic numerical model using an iterative approach. As the rock core is partially fractured due to previous face advance blasting, the numerical model is further adjusted to model the observed damage zone. The 3D model after adjustments is used to examine the mining front stability with the Hoek–Brown failure criterion. It is postulated that the proposed methodology is suitable for the stability assessment of any mining front with or without an observed damage zone.

Keywords: mining front stability assessment; diametrical core deformation technique; local field stresses; stress field distribution



Citation: Li, Y.; Mitri, H.S. Practical Methodology for Evaluating Mining Front Stability Based on the Diametrical Core Deformation Technique. *Minerals* **2024**, *14*, 385. <https://doi.org/10.3390/min14040385>

Academic Editor: Elsabe Kearsley

Received: 15 February 2024

Revised: 21 March 2024

Accepted: 5 April 2024

Published: 8 April 2024



Copyright: © 2024 by the authors. Licensee MDPI, Basel, Switzerland. This article is an open access article distributed under the terms and conditions of the Creative Commons Attribution (CC BY) license (<https://creativecommons.org/licenses/by/4.0/>).

1. Introduction

As mine development and production activities continue, mining front stresses in drifts, ramps, and sill drives keep on changing. Such dynamic changes could significantly influence the stability of the mining front, leading to one of various forms of rock failure. Therefore, many research efforts have been focused on studying mining-induced stress, e.g., [1–5]. Such studies, however, have primarily employed a single study approach, such as numerical simulation, theoretical analysis, or field testing. In this study, the estimation of mining-induced stress distribution and mining front stability is performed through a combination of field work, laboratory measurements, and numerical modelling. The significance of the proposed methodology lies in the use of actual in situ data that are precisely measured in laboratory. The measurements are then used as input parameters in a theoretical model for mining front stress estimation at the point of the in situ experiment. Finally, the estimated stress information obtained from this procedure is used to calibrate the numerical model of the mining front, enabling the prediction of the complete stress distribution and the assessment of the front stability.

The principal stresses in the plane parallel to the mining front can initiate face failure by triggering different failure mechanisms, such as spalling, slabbing, burst, bulking and out-of-plane shear failure [6,7]. In deep mining, these planar stresses could cause immediate failure, even rockburst, during mining, especially in brittle rock [8]. Consequently, it is important to regularly assess the mining front stability.

This research proposes a practical methodology for mining front stability evaluation using the diametrical core deformation technique (DCDT) and numerical modelling. DCDT, a recently developed technique by the authors for determining mining-induced planar stresses based on the diametrical core deformations [9], relies on measuring the stress relief of rock cores to estimate the induced stress at the point of core extraction. Such relief can be captured in laboratory through a custom-designed core diameter measuring system [10]. Numerical modelling is employed to simulate the conditions near the access drift of the case study at the Eleonore mine in northern Quebec, Canada.

In this case study, a rock core was retrieved from the face of an access drift on the 530 level. A portion of the intact rock obtained at 2.5 m from the face was used to conduct the DCDT, facilitating the determination of planar principal stresses, both in terms of magnitude and orientation. Subsequently, the DCDT results were used to adjust the local stress orientation and magnitude in a 3D numerical model to obtain a complete stress distribution over the mining front. The Hoek–Brown failure criterion was then selected in the numerical model to complete the stability analysis of the mining face. The choice of the failure criterion is one that is made by the analyst and has no bearing on the validity of the proposed methodology.

2. Case Study Mine

Eleonore is a gold mining operation in northern Quebec, Canada, owned by Newmont Corporation. The Eleonore deposit is located under the Opinaca reservoir; it outcrops to surface in the Roberto area and extends 1.9 km along the strike and over at least 1400 m below surface. The projected production rate is 270,000 oz per year using a longhole open stoping mining method. The footwall developments are driven in thinly bedded wacke, sporadically traversed by pegmatite dykes and quartz veins and veinlets. The case study drift is situated 530 m below the surface.

Field and laboratory investigations of the mechanical properties of the rockmass were commissioned by Eleonore Mine in 2008. The results of the uniaxial compressive strength (UCS), tensile strength (σ_t), Young's modulus of elasticity for intact rock (E_i), Young's modulus of elasticity for rockmass (E_{rm}), Poisson's ratio (ν), and Hoek–Brown's m_i parameter for intact rock, are listed in Table 1. The mechanical properties of the intact rock (which were used for DCDT calculations) and the rockmass properties of the wacke rock, which were used for numerical modelling.

Table 1. Geomechanical properties in the case study area.

Rock Type	UCS (MPa)	σ_t (MPa)	Density (g/cm ³)	E_i (GPa)	E_{rm} (GPa)	ν	m_i	RMR ₇₆
Wacke	162	15	2.75	39.05	28.62	0.14	11	70–84

There are several in situ stress measurements that have been conducted at Eleonore; the maximum principal stress is generally in E-W and the local maximum stress varies to the direction that perpendicular to folds of the orebody [11]. Stress conditions are given as follows:

$$\begin{aligned}\sigma_1^0 &= 19 + \gamma z \\ \sigma_2^0 &= \gamma z \\ \sigma_3^0 &= \gamma z\end{aligned}\quad (1)$$

where σ_1^0 is the maximum horizontal in situ stress and σ_2^0 is the minimum horizontal stress; σ_3^0 is the vertical in situ stress; γ is the rock unit weight, equal to 0.0275 MN/m³ for the wacke formation; and z is the depth.

3. Diametrical Core Deformation Technique

3.1. Rock Core Extraction

The rock core was extracted using a diamond drill and oriented perpendicular to the front of 0530-AMN-509 access drift shown in Figure 1. The drift is 5 m × 5 m and is found

in wacke rock formation (see Figure 2). The rock core is 3 m long and was drilled off with NQ (47.6 mm I.D.) diamond drill bit. As can be seen from the photo in Figure 3, the rock core is severely damaged in the first 2.5 m with visible fragmentation. As the method of face advance at the mine is by traditional drilling and blasting with explosive energy, the observed damage in the extracted core is attributed to blast vibrations from the previous blast round. Modelling of the damage zone will be discussed in a later section. The intact rock obtained from 2.5 m to 3 m was used for conducting the DCDT. The gravity direction was marked on the rock core, which allowed us to determine the stress orientation in the laboratory with respect to gravity.

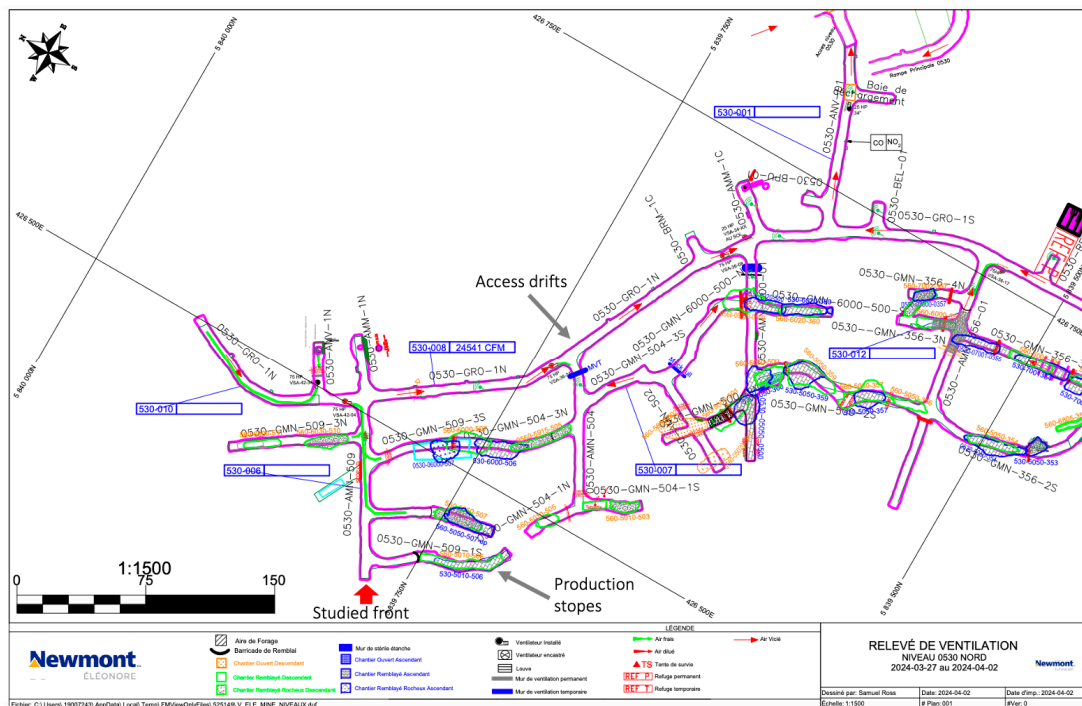


Figure 1. Plan view of Eleonore mine 530 level—studied front location.

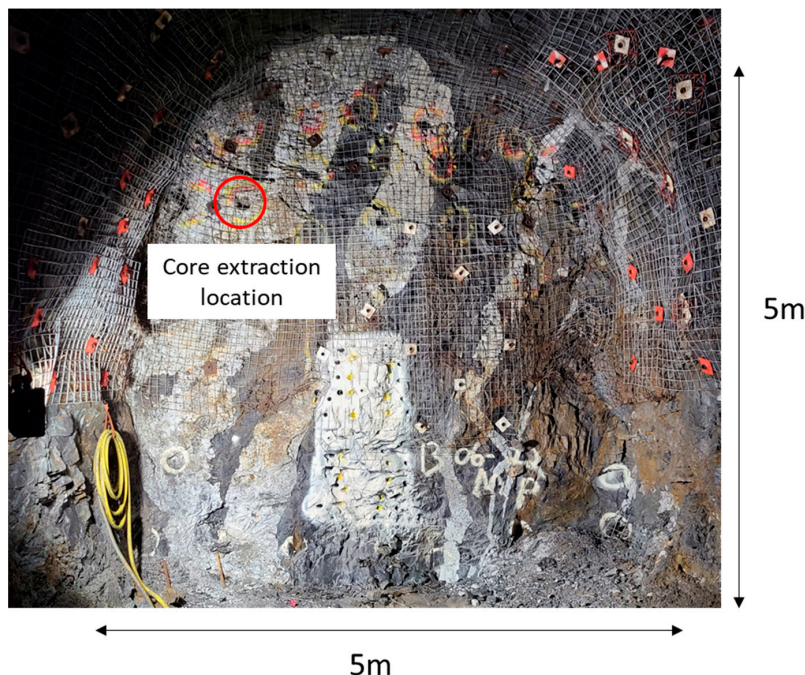


Figure 2. Location of core extraction on 0530-AMN-509 access drift.

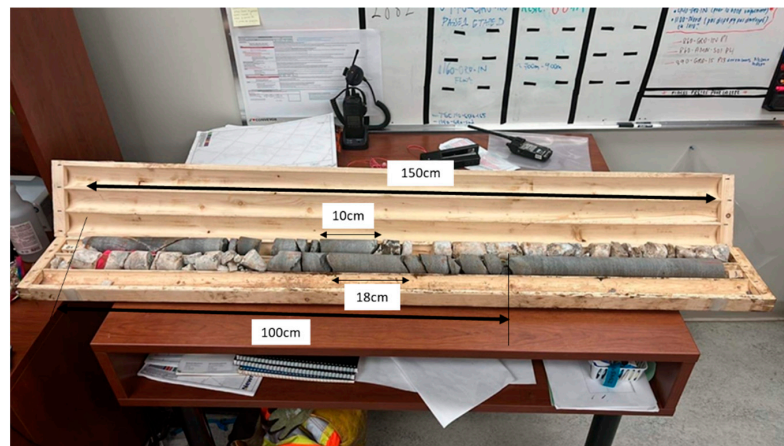


Figure 3. Extracted rock core.

3.2. Diametrical Core Deformations

The round shape of the rock core changes once it is drilled off, due to stress relief. Such a shape change is a function of the biaxial stresses acting in the plane perpendicular to the borehole axis and parallel to the mining face as shown in Figure 4. The underlying hypothesis of the DCDT is that the rock behaves as a linear elastic material. The principal stress orientation can be easily determined once the maximum and minimum diameters d_{max} and d_{min} are identified, which also represent the directions of the local major and minor principal stresses. To obtain accurate results, the core diameters are measured using a high precision customized test apparatus [10].

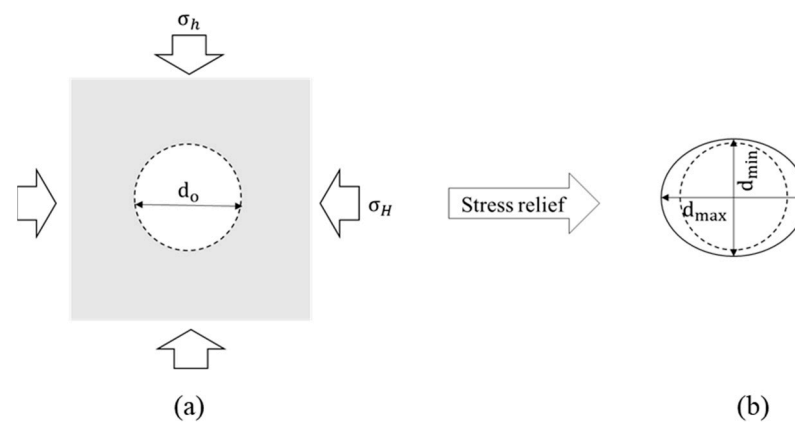


Figure 4. Schematic of rock core relief, (a) core before drilling; (b) extracted core [12].

Rock core deformations were measured over a complete turn of 360° with a customized apparatus including a laser micrometer having a resolution of 0.0001 mm (Figure 5). Measurements were repeated at three adjacent locations along the core and the results are best fitted with sinusoidal curves as shown in Figure 6. The average measured maximum and minimum diameters are: $d_{max} = 47.1950$ mm and $d_{min} = 47.1604$ mm.



Figure 5. Measurement apparatus of diametrical core deformation.

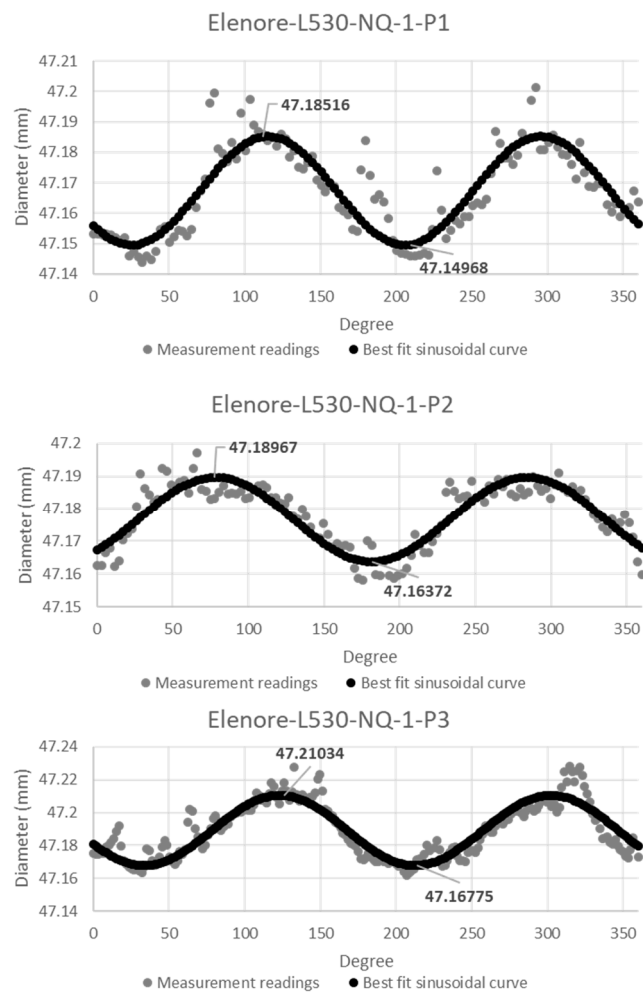


Figure 6. Diametrical core measurement results.

3.3. Estimation of Mining Front State of Stress

The analytical model of the DCDT [9] is derived based on linear elastic rock core deformation due to strain relief, which is a function of the surrounding stress field and the modulus elasticity of the rock. To use the analytical model of the DCDT for mining front principal stress calculation, the intact rock properties (E, ν) of the wacke in Table 1 are used along with the measured core diameters. The results show that the estimated local principal stresses σ_L and σ_l that, in the plane perpendicular to the borehole axis, are 25.0 MPa and 3.5 MPa, respectively, when the stress along the core axis $\sigma_x = 0$. These values will be updated using the following generalized analytical model once σ_x is computed from the numerical model [9]:

$$\frac{1}{E} \{ \sigma_L - \nu(\sigma_l + \sigma_x) \} = \frac{d_{max} - d_o}{d_o} \tag{2a}$$

$$\frac{1}{E} \{ \sigma_l - \nu(\sigma_L + \sigma_x) \} = \frac{d_{min} - d_o}{d_o} \tag{2b}$$

$$d_o = \sqrt{\frac{(3d_{max}^2 + 3d_{min}^2 + 2d_{max}d_{min}) \left[1 + \frac{1}{E} [\sigma_x - \nu(\sigma_L + \sigma_l)] \right]}{\left(\frac{1-2\nu}{E} (\sigma_L + \sigma_l + \sigma_x) + 1 \right)}} \tag{2c}$$

where d_o is the original core diameter before stress relief.

It is noteworthy that the state of stress is naturally plane stress at the free face ($\sigma_x = 0$). In this case, the DCDT equations will directly calculate σ_L and σ_l at the face. However, behind the mining face ($x > 0$), the stress component $\sigma_x > 0$, in which case the state of stress is three-dimensional, and there is a need to estimate σ_x at the point of interest in order to estimate σ_L and σ_l from Equation (2).

The results also show that the orientation of the minor principal stress σ_l —representing gravity—is subvertical, as it is 10° clockwise from gravity, as shown in the photo of Figure 7.

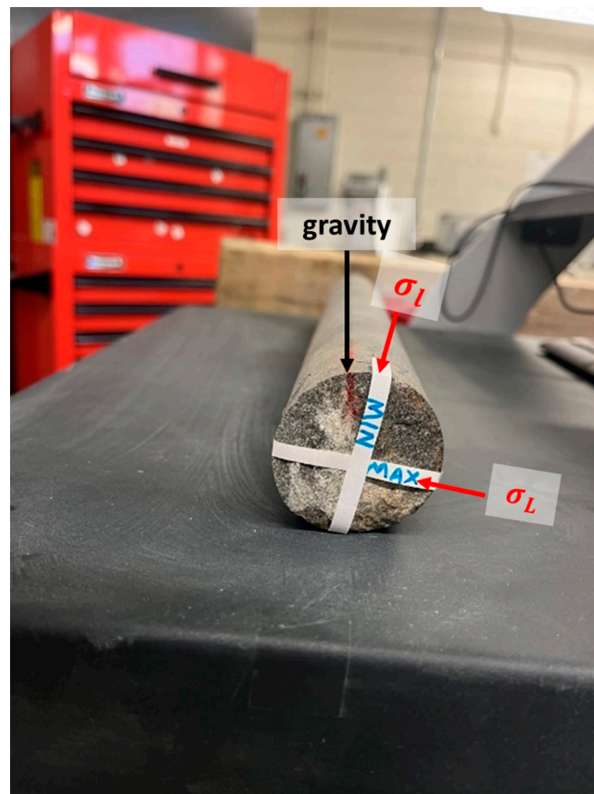


Figure 7. Determination of stress orientation from DCDT.

Based on these results, it can be postulated that the local principal stress magnitudes and orientation in the YZ plane of the access drift face are as shown in Figure 8. As the access drift axis is perpendicular to the ore vein (Figure 1) and, according to Hauta et al. (2020), the major principal in situ stress σ_1^0 is parallel to the drift axis. It is noteworthy that σ_1^0 becomes naturally zero at the free mining face, i.e., on the local scale, it is the minor principal stress at the drift face.

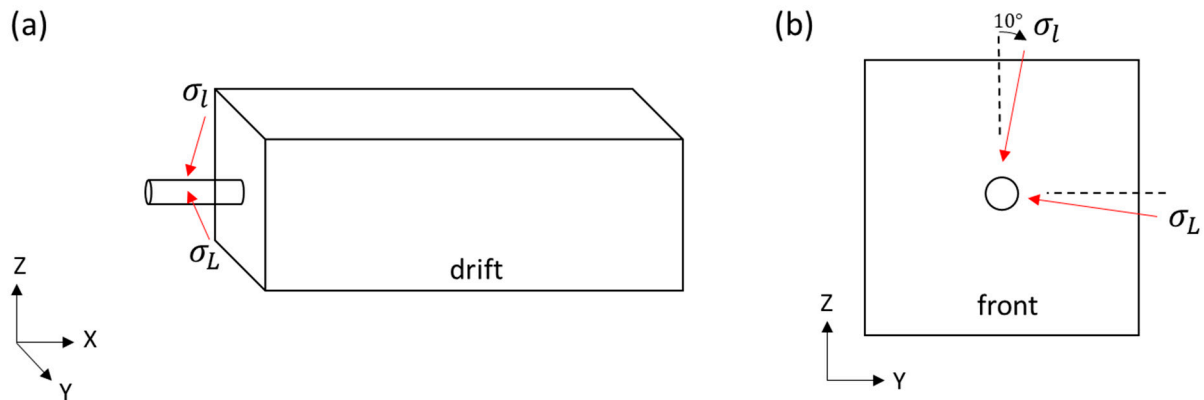


Figure 8. State of stress near the mining front, (a) stresses in three directions on a borehole; (b) cross-sectional view of the borehole showing principal stresses.

Clearly, these results would have been further validated had more rock cores been retrieved from the drift face. In future, more rock cores should be drilled off for better estimation of the stress state using the DCDT.

4. Numerical Modelling

As core deformation measurements took place only at one point in the drift face, it is not sufficient to assess the overall stability of the face. Therefore, it is deemed necessary to create a 3D numerical model to simulate the access drift and its mining front. The model is 50 m × 50 m × 50 m, with a 5 m × 5 m drift that is 25 m long. Roller boundaries are applied to all six faces of the model, and the top boundary is 505 level and the drift is at 530 level as shown in Figure 9. The model is built with Rhino CAD software and solved with finite difference code FLAC3D. The rockmass properties of the wacke formation are listed in Table 1, and the in situ stress regime from the measurement is adopted from Equation (1). The model is run in linear elastic mode. Based on the core deformation results, the orientation of σ_3^0 in Equation (1) is rotated 10° clockwise from vertical in the numerical model (as shown in Figure 8). Model sensitivity analysis of mesh sizes was carried out for more accurate computation of stress results around the drift opening. In the sensitivity analysis, the mesh density is increased in each model and the displacement in the X-direction at the center of the face is recorded. Displacement convergence is observed with a refined mesh size of 0.075 m near the mining front, resulting in a total number of 929,042 zones in the 3D model.

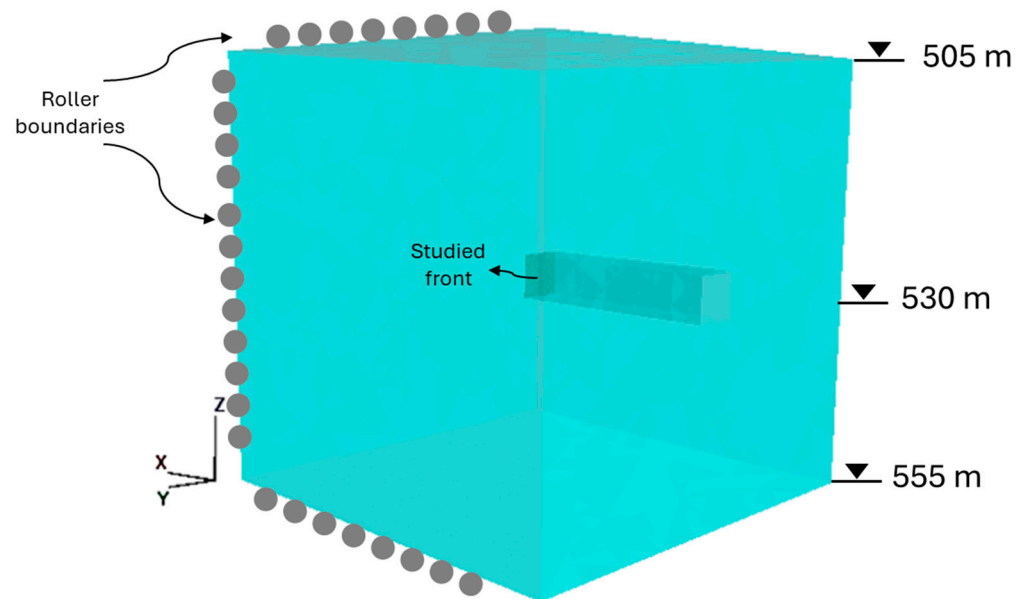


Figure 9. Illustration of FLAC3D model.

5. Modelling of Damage Zone

When a damage zone is identified in the rock core, as is in this study, damage properties should be estimated and simulated in the numerical model. The following is a proposed simple procedure to account for the damage zone. As fracturing of the rock core is attributed to blasting of the previous round, it is proposed to treat the damage zone using the constitutive model for panel destressing proposed by [13]. In their work, the destress panel is modeled with a rock fragmentation factor, α , and a stress dissipation factor, β , whereby:

$$E_{\text{destress}} = E\alpha \quad (3)$$

where E_{destress} is the destressed modulus of elasticity, and the factor α ranges from 0 to 1.

The Poisson's ratio (ν) is modified as follows [14]:

$$\nu_{\text{destress}} = \nu(2 - \alpha) \quad (4)$$

Finally, the stress dissipation factor β is used to obtain the residual stress tensor (σ_r) in the destressed zone and is given by

$$\{\sigma_r\} = (1 - \beta)\{\sigma\} \quad (5)$$

where the factor β ranges from 0 to 1.

Based on [13], the values of $\alpha = 0.4$, $\beta = 0.6$ are adopted in the damage zone. The numerical model can now be solved with the drift excavation and damage zone simulated as illustrated in Figure 10.

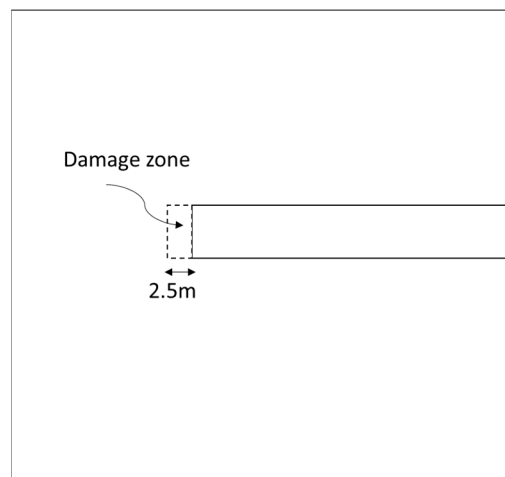


Figure 10. Schematic of the model with damage zone.

6. Adjustment of In Situ Stress

The numerical model is first initialized with the rotated in situ stress field defined in Equation (1), and after equilibrium is reached, the drift excavation and damage zone are simulated. The computed stresses at four observation points along an axis passing through the extracted core location in the drift face are listed in Table 2. The points are located on the drift face and 2 m, 2.5 m, and 3 m behind the face. As expected, σ_x at the mining front is nearly zero, gradually increasing to 15.5 MPa behind the face. The remaining stress components σ_y , σ_z , and τ_{yz} can be transformed to principal stresses σ_L^C, σ_I^C in the YZ plane. These are listed in Table 2.

Table 2. FLAC3D stress results in MPa at and behind the mining front.

Location	Face	2 m	2.5 m	3 m
σ_x	0.2	8.7	12.0	15.5
σ_y	2.8	2.9	14.7	17.0
σ_z	2.8	3.0	14.7	16.6
τ_{yz}	0.36	−0.80	−0.89	−1.36
σ_L^C	3.2	3.8	15.6	18.2
σ_I^C	2.4	2.1	13.8	15.4

The DCDT stresses can now be updated with the stress $\sigma_x = 12$ MPa at 2.5 m where intact core was found and measured. Thus, according to Equations (2a)–(2c), the DCDT stresses (σ_L, σ_I) become 33.6 MPa and 6 MPa, respectively.

To match the computed stresses (σ_L^C, σ_I^C) with those estimated from the DCDT (σ_L, σ_I), an iterative stress adjustment process is required. As the DCDT was applied at a depth of 2.5 m to 3 m due to rock core damage in the first 2.5 m, the results from FLAC3D at that depth are queried and considered for comparison with the DCDT results. The magnitudes of the initial in situ stresses σ_2^0 and σ_3^0 are varied iteratively until the results are within 10% of the DCDT values. Similarly, the iteration of orientation adjustment starts with the initialized directions of σ_2^0 and σ_3^0 , and finishes off when computed stress σ_I^C at 2.5 m is in the same direction as σ_I obtained from DCDT. The stress iteration results are listed in Table 3. Note that the in situ stress field in the X-direction remains unchanged (Equation (1)).

Table 3. Iteration results of stress adjustment.

Iteration	Initial In Situ Stress			FLAC3D Computed at 2.5 m						
	σ_2^0 (MPa)	σ_3^0 (MPa)	θ^0 * (°)	σ_L^C (MPa)	σ_1^C (MPa)	θ^C * (°)	σ_x (MPa)	σ_y (MPa)	σ_z (MPa)	τ_{yz} (MPa)
1	14.6	14.6	10	15.6	13.8	45	12.0	14.7	14.7	−0.9
2	26.3	14.6	10	31.4	14.3	−6.2	12.5	31.2	14.5	1.8
3	26.3	8.8	10	31.6	5.5	−8.2	12.2	31.1	6.1	3.7
4	26.3	9.5	10	31.6	6.6	−8.1	12.2	31.1	7.1	3.5
5	26.3	9.5	−8.1	32.9	6.3	11.3	12.4	31.9	7.3	−5.1

* θ^0 is the initialized major principal stress orientation; θ^C is the FLAC3D commutated major principal stress orientation.

By applying the iterative stress adjustment, the FLAC3D model results should closely match the stress components estimated from the core deformation measurements and the analytical model. The numerical model is re-solved iteratively with the updated in situ stress regime. The updated local stress regime is $\sigma_L = 26.3$ MPa, $\sigma_1 = 9.5$ MPa, and along drift stress stays the same ($\sigma_x = 12$ MPa). As can be seen from the comparison of stress results from FLAC3D and the DCDT, there is a difference of approximately 5% or less between the results (Table 4) after five iterations were made. As the process is iterative, it must end with a margin of difference between the FLAC3D and DCDT results. An acceptable difference may be considered as one that will not significantly change the outcome of the analysis. In this study, a change of 5% in the local stress, σ_L , did not influence the stress results in the mining front. Therefore, such margin of error is deemed acceptable for all practical reasons.

Table 4. Comparison of stress results at the location of extracted core.

Stress (MPa)	FLAC3D	DCDT	Difference%
σ_L	32.9	33.6	2.1%
σ_1	6.3	6.0	5%

Now, the full-face state of stress behind the damage zone can be extracted from FLAC3D. Figure 11 displays the normal stress distribution in the YZ plane behind the damage zone. The mining front stability is assessed by the Factor of Safety (FS) based on the [15,16]. In the present study, the FS is estimated by calculating the strength to the applied stress ratio measured from the hydrostatic line $\sigma_1 = \sigma_3$ as follows.

$$FS = \frac{[\sigma_3 + (m\sigma_{ci}\sigma_3 + s)^{0.5}] - \sigma_3}{\sigma_1 - \sigma_3} \tag{6}$$

where m and s are the material constants; σ_{ci} is the unconfined compressive strength. It is noteworthy that the calculation of the Factor of Safety (FS) in this study is simply the strength divided by the applied stress, whereby both quantities are measured from the hydrostatic line of $\sigma_1 = \sigma_3$. While there is more than one method to estimate factors of safety (e.g., [17–19]), the notion of measuring strength and applied stress from the hydrostatic line is not uncommon in practice. The choice of a threshold below which the FS is considered to indicate local failure is one that is decided by the analyst.

Figure 12 shows the FS results behind the face. In general, this mining front is considered stable, except for a few areas. It is also observed that the FS distribution is not symmetrical. This is due to the oblique orientation that the mining face makes with the rotated in situ stresses σ_2^0 and σ_3^0 , as discussed before.

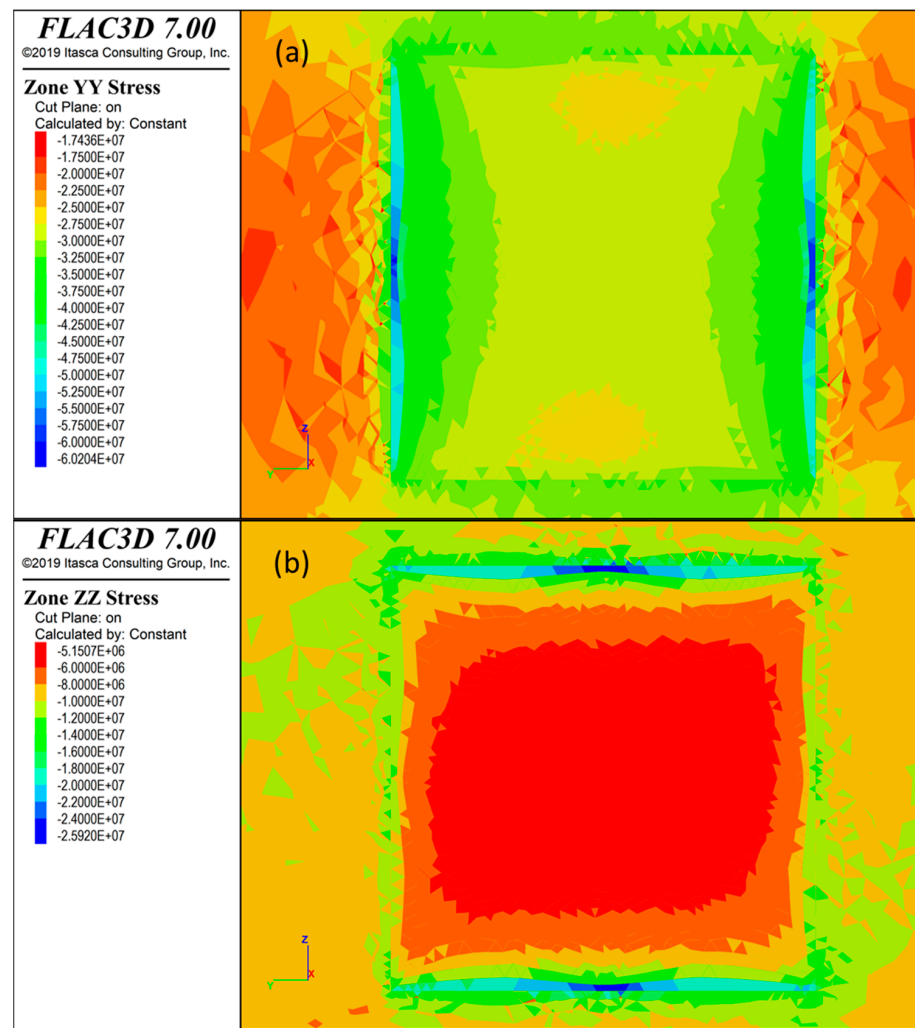


Figure 11. Stress distribution behind damage zone; (a) σ_y distribution (b) σ_z distribution.

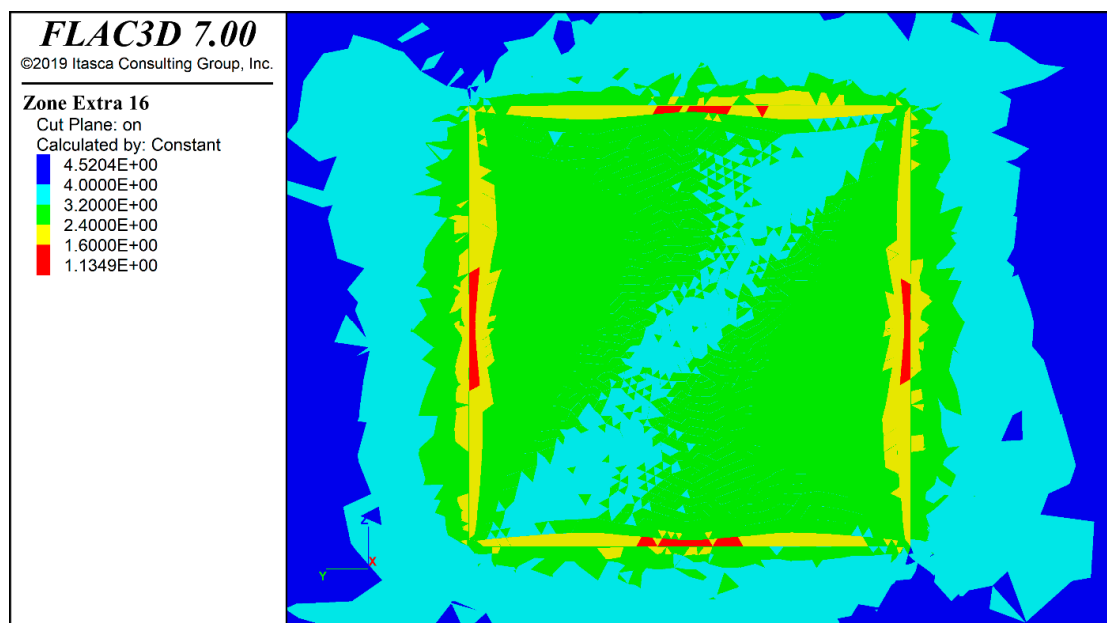


Figure 12. Factor of safety for the front behind damage zone.

7. Conclusions

This study describes a practical methodology for assessing mining face stability. It involves the retrieval of one or more rock cores from the mining face and measuring their diametrical deformations using a high precision laser measurement apparatus with a resolution of 0.1 micrometer. The state of local principal stresses in a plane perpendicular to the core axis can then be estimated using the DCDT. The state of stress is naturally plane stress at the free face ($\sigma_x = 0$). In this case, the DCDT equations will directly calculate the principal stress components σ_L and σ_I at the free face. However, behind the mining face ($x > 0$), the stress component $\sigma_x > 0$, in which case the state of stress is three-dimensional, and there is a need to estimate σ_x at the point of interest to estimate σ_L and σ_I from Equation (2). A local 3D numerical model is built and adjusted to match the stress components estimated by the DCDT and their orientation. The adjustments allow the numerical model to produce full-face stress distribution for stability assessment. The methodology used a case study mine in northern Quebec, where a wacke rock core was extracted from an access drift situated 530 m below surface. As blast-induced damage was observed in the rock core, a destress blasting constitutive model from previous studies was adopted to model the damage zone using two model parameters, namely the rock fragmentation factor α and stress dissipation factor β . The depth of the damage zone is determined by the observation that the rock core is fragmented within the first 2.5 m. Thus, the extent of the damage zone is approximated to the length of 2.5 m for the drift face. The Hoek–Brown failure criterion is selected to demonstrate face stability assessment with a factor of safety calculation after the linear elastic analysis. The calculation of the FS in this study is simply estimated by the strength divided by the applied stress, whereby both quantities are measured from the hydrostatic line of $\sigma_1 = \sigma_3$. While there is more than one method to estimate factors of safety for criteria such as Mohr–Coulomb and Hoek–Brown, the notion of measuring strength and applied stress from the hydrostatic line is not uncommon in practice. The choice of a threshold below which the FS is considered to indicate local failure is one that is decided by the analyst. The findings of this study indicate that DCDT can be a practical tool for the assessment of mining face stability especially when coupled with numerical modelling. For future studies, it is recommended that more rock cores be drilled in the mining front and used in the DCDT. For example, by drilling four rock cores from the drift face, a richer dataset of stress information can be generated from the DCDT, potentially enhancing the reliability of the numerical model capability of predicting the mining front stress distribution and stability.

Author Contributions: Conceptualization, Y.L.; methodology, Y.L.; software, Y.L.; validation, Y.L.; formal analysis, Y.L.; investigation, Y.L.; resources, Y.L.; data curation, Y.L.; writing—original draft preparation, Y.L.; writing—review and editing, Y.L.; visualization, Y.L.; supervision, H.S.M.; project administration, H.S.M.; funding acquisition, H.S.M. All authors have read and agreed to the published version of the manuscript.

Funding: This work was funded by Natural Resources Canada, Clean Growth Program, Grant No. CGP-17-1003 and industry partner Newmont Corporation. The authors are grateful for their support.

Data Availability Statement: The research data presented in the present paper is available from the corresponding author upon request due to privacy.

Conflicts of Interest: The authors declare no conflicts of interest.

References

1. Singh, A.K.; Singh, R.; Maiti, J.; Kumar, R.; Mandal, P.K. Assessment of mining induced stress development over coal pillars during depillaring. *Int. J. Rock Mech. Min. Sci.* **2011**, *48*, 805–818. [[CrossRef](#)]
2. Singh, R.; Singh, A.K.; Maiti, J.; Mandal, P.K.; Singh, R.; Kumar, R. An observational approach for assessment of dynamic loading during underground coal pillar extraction. *Int. J. Rock Mech. Min. Sci.* **2011**, *48*, 79. [[CrossRef](#)]
3. Shabanimashcool, M.; Li, C.C. Numerical modelling of longwall mining and stability analysis of the gates in a coal mine. *Int. J. Rock Mech. Min. Sci.* **2012**, *51*, 24–34. [[CrossRef](#)]

4. Shabanimashcool, M.; Li, C.C. A numerical study of stress changes in barrier pillars and a border area in a longwall coal mine. *Int. J. Coal Geol.* **2013**, *106*, 39–47. [[CrossRef](#)]
5. Li, S.; Gao, M.; Yang, X.; Zhang, R.; Zhang, Z.; Li, G.; Zhang, Z.; Xie, J. Numerical simulation of spatial distributions of mining-induced stress and fracture fields for three coal mining layouts. *J. Rock Mech. Geotech. Eng.* **2018**, *10*, 907–913. [[CrossRef](#)]
6. Ortlepp, D.W. *Rock Fracture and Rockbursts: An Illustrative Study*; South African Institute of Mining and Metallurgy: Johannesburg, South Africa, 1997.
7. Ortlepp, D.W.; Stacey, T.R. Rockburst mechanisms in tunnels and shafts. *Tunneling Undergr. Space Technol.* **1994**, *9*, 59–65. [[CrossRef](#)]
8. Yun, X.; Mitri, H.S.; Yang, X.; Wang, Y. Experimental investigation into biaxial compressive strength of granite. *Int. J. Rock Mech. Min. Sci.* **2010**, *47*, 334–341. [[CrossRef](#)]
9. Li, Y.; Mitri, H.S. Methodology for the estimation of mining face stresses using rock core diametrical deformation. *Int. J. Rock Mech. Min. Sci.* **2023**, *161*, 105300. [[CrossRef](#)]
10. Li, Y.; Mitri, H.S. Determination of mining-induced stresses using diametral rock core deformations. *Int. J. Coal Sci. Technol.* **2022**, *9*, 80. [[CrossRef](#)]
11. Hauta, R.L.; Rebuli, D.B.; Meyer, S. Back-analysis of a stope failure using seismic and geotechnical data. In Proceedings of the 54th US Rock Mechanics/Geomechanics Symposium 2020, Golden, CO, USA, 28 June–1 July 2020, ARMA 20-1904.
12. Funato, A.; Ito, T. A new method of diametrical core deformation analysis for in-situ stress measurements. *Int. J. Rock Mech. Min. Sci.* **2017**, *91*, 112–118. [[CrossRef](#)]
13. Vennes, I.; Mitri, H.S.; Chinnasane, R.D.; Yao, M. Large-scale destress blasting for seismicity control in hard rock mines: A case study. *Int. J. Min. Sci. Technol.* **2020**, *30*, 141–149. [[CrossRef](#)]
14. Tang, B.; Mitri, H.S. Numerical modelling of rock preconditioning by destress blasting. *Proc. Inst. Civ. Eng.-Ground Improv.* **2001**, *5*, 57–67. [[CrossRef](#)]
15. Hoek, E.; Brown, E.T. Practical estimates of rock mass strength. *Int. J. Rock Mech. Min. Sci.* **1997**, *34*, 1165–1186. [[CrossRef](#)]
16. Hoek, E.; Brown, E.T. *Underground Excavations in Rock*; Institution of Mining and Metallurgy: London, UK, 1980.
17. Shoerey, P.R.; Biswas, A.K.; Choubey, V.D. An empirical failure criterion for rocks and jointed rock masses. *Eng. Geol.* **1989**, *26*, 141–159. [[CrossRef](#)]
18. Yudhbir, Y.; Lemanza, W.; Prinzl, F. An Empirical Failure Criterion for Rock Masses. In Proceedings of the 5th ISRM Congress, Melbourne, Australia, 10–15 April 1983.
19. Bieniawski, Z.T. Estimating the strength of rock materials. *J. South. Afr. Inst. Min. Metall.* **1974**, *74*, 312–320. [[CrossRef](#)]

Disclaimer/Publisher’s Note: The statements, opinions and data contained in all publications are solely those of the individual author(s) and contributor(s) and not of MDPI and/or the editor(s). MDPI and/or the editor(s) disclaim responsibility for any injury to people or property resulting from any ideas, methods, instructions or products referred to in the content.